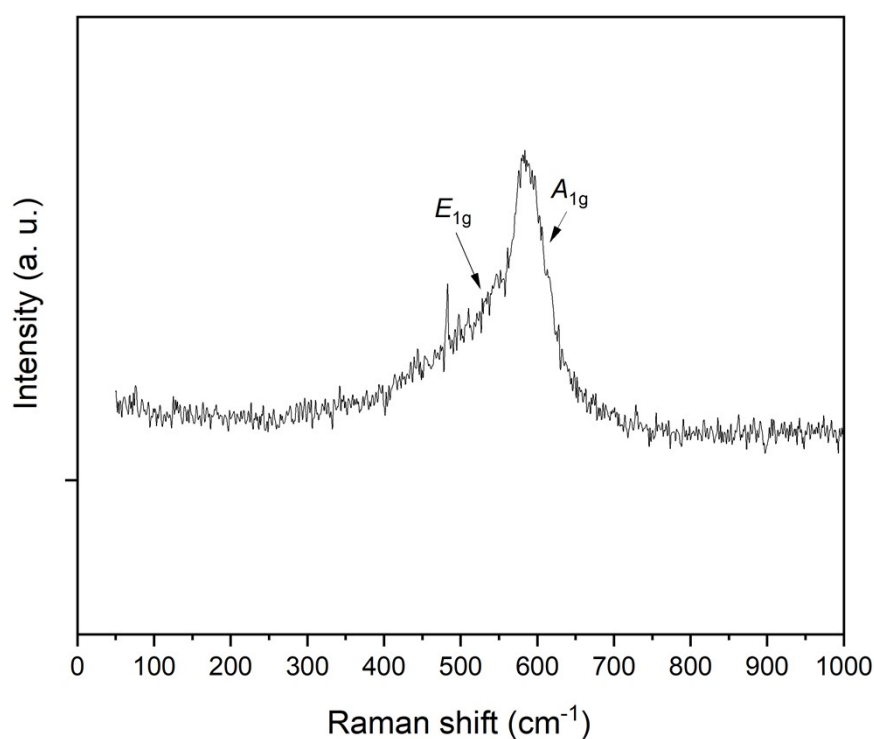


**Impact of O3/P3 phase transition on the performance  
of  $\text{Na}_x\text{Ti}_{1/6}\text{Mn}_{1/6}\text{Fe}_{1/6}\text{Co}_{1/6}\text{Ni}_{1/6}\text{Cu}_{1/6}\text{O}_2$  cathode material for Na-ion batteries**

Fig. 1 presents a Raman spectrum recorded for the  $\text{Na}_1\text{Ti}_{1/6}\text{Mn}_{1/6}\text{Fe}_{1/6}\text{Co}_{1/6}\text{Ni}_{1/6}\text{Cu}_{1/6}\text{O}_2$  LT830 oxide. In the presented spectrum, two bands specific to the hexagonal  $R\text{-}3m$  O3-phase can be seen [1]. The shift of the  $E_{1g}$  band towards higher energies, into the area of the  $A_{1g}$  band, corresponds to the relatively high parameter value obtained based on XRD measurements [1, 2].



**Fig. 1S.** Raman spectrum recorded for the LT830  $\text{Na}_1\text{Ti}_{1/6}\text{Mn}_{1/6}\text{Fe}_{1/6}\text{Co}_{1/6}\text{Ni}_{1/6}\text{Cu}_{1/6}\text{O}_2$  oxide.

Fig. 2S presents a FTIR spectrum recorded for the  $\text{Na}_1\text{Ti}_{1/6}\text{Mn}_{1/6}\text{Fe}_{1/6}\text{Co}_{1/6}\text{Ni}_{1/6}\text{Cu}_{1/6}\text{O}_2$  LT830 oxide. In the presented spectrum, wide band with maximum at  $559\text{ cm}^{-1}$  can be observed. The second, poorly defined band can be seen around  $480\text{ cm}^{-1}$ . The bands in this range are

typical for skeletal vibrations of the oxygen-central metal bonds [3, 4]. Due to the substitution of the central site with six different *3d* atoms, the signals are strongly broadened.

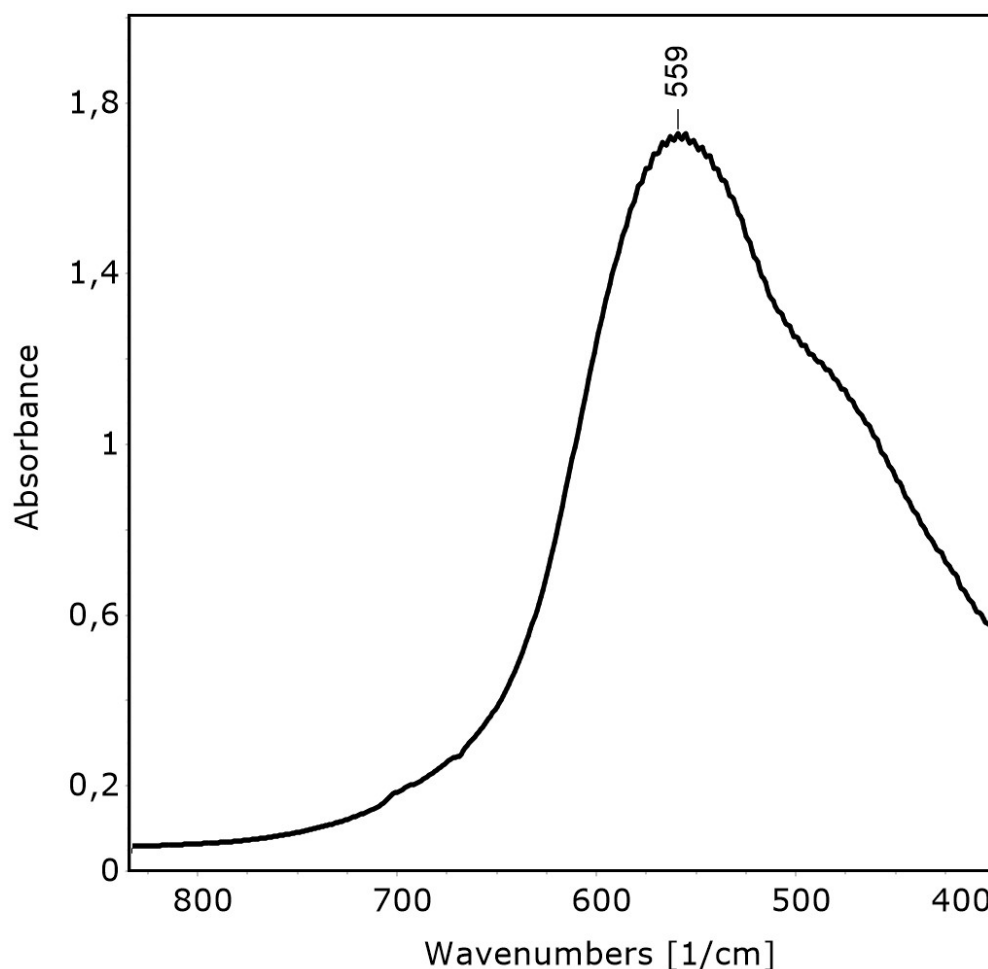


**Fig. 2S.** FTIR spectrum recorded for the LT830  $\text{Na}_1\text{Ti}_{1/6}\text{Mn}_{1/6}\text{Fe}_{1/6}\text{Co}_{1/6}\text{Ni}_{1/6}\text{Cu}_{1/6}\text{O}_2$  oxide.

Long-cycling performance was investigated for both LT830 and HT900 oxides using as cathodes (Fig. 3S). Batteries were cycled with current 1C. In both cases the initial discharge capacities achieved values which were similar to those presented in Fig. 3a. Unfortunately, the discharge capacity decreased rapidly with successive cycles. This can be explained taking into account poor conductivity of the O3 phase and the unfavourable volume changes of the P3/O3 phase transition.

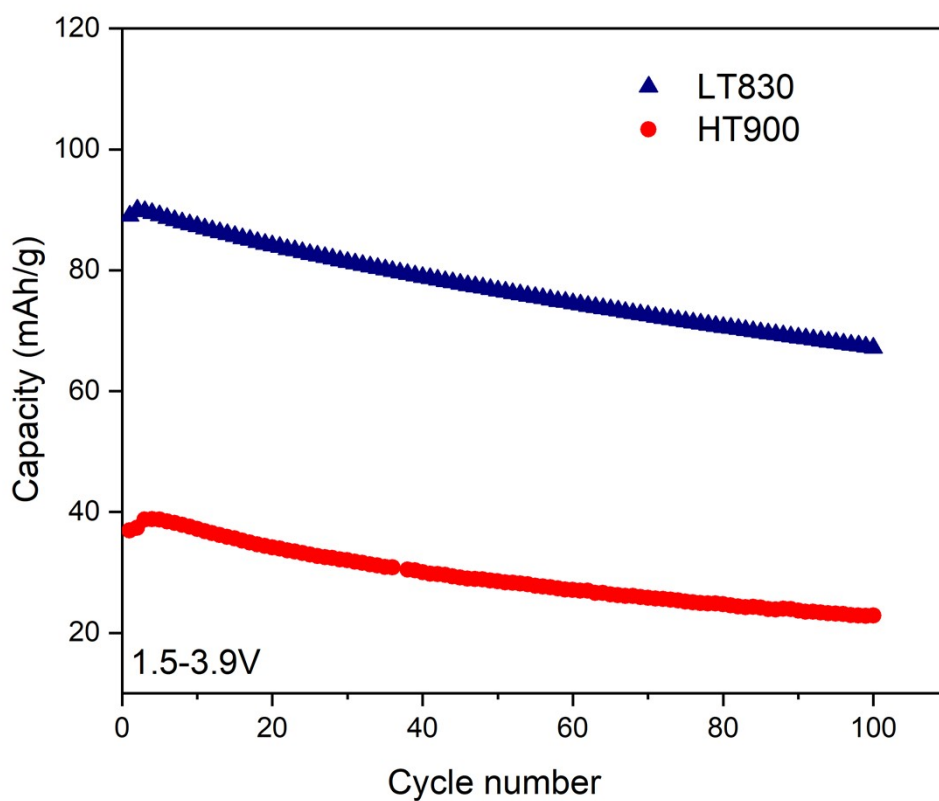
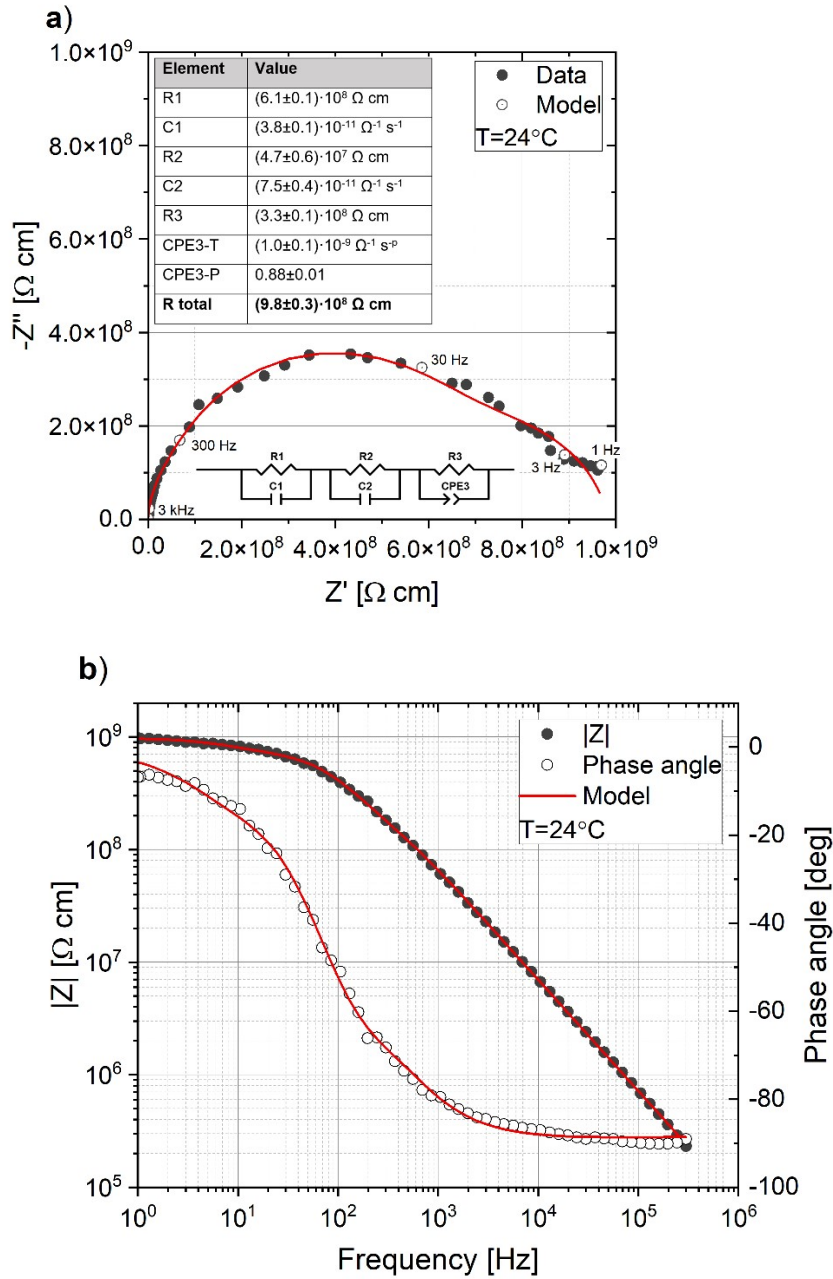


Fig. 3S. Long-cycling performance conducted for both LT830 and HT900 oxides using as cathodes.

Fig. 4S presents Nyquist and Bode plots of the frequency response of the HT900  $\text{Na}_1\text{Ti}_{1/6}\text{Mn}_{1/6}\text{Fe}_{1/6}\text{Co}_{1/6}\text{Ni}_{1/6}\text{Cu}_{1/6}\text{O}_2$  sintered sample with sputtered gold electrodes. The relative density of the sinter was approx. 65%, which makes the absolute value of the estimated electrical conductivity imprecise. Nevertheless, the results can be used to discuss general trends and the character of electrical conductivity.



**Fig. 4S.** (a) Nyquist and (b) Bode plots of frequency response for  $\text{Na}_1\text{Ti}_{1/6}\text{Mn}_{1/6}\text{Fe}_{1/6}\text{Co}_{1/6}\text{Ni}_{1/6}\text{Cu}_{1/6}\text{O}_2$  HT900 with Au electrodes at  $24^\circ\text{C}$ . Inset in plot (a) presents the applied equivalent circuit and refined parameters of the impedance model.

The recorded impedance spectrum was modelled using the equivalent circuit presented as an inset in Fig. 4Sa. At least three relatively similar time constants were necessary to properly reproduce the shape of the spectrum and the refined parameters of the equivalent circuit are

listed in a table inserted in the same figure. At this moment, the origin of the multiple time constants remains unexplained and requires further investigations, but it may be conjectured that they are related to complex microstructural features or to mixed ionic-electronic mechanism of electrical conductivity. It should be noted that the shape of the low frequency part of the measured impedance spectrum indicates that the Au electrodes were non-blocking, and therefore sodium ions cannot be considered the predominant charge carriers. Even given that the origin of the impedance response is not fully clarified, total electrical resistance can be deduced from the low frequency part of the spectrum, where resistance approaches  $9.8 \cdot 10^8 \Omega$  cm. Total electrical conductivity of the sample could thus be estimated to be  $1.0 \cdot 10^{-9} \text{ S cm}^{-1}$ , which is a surprisingly low compared with the values reported for other simple O3-type layered oxides [5].

To gain better insight into the mechanism of charge transport in this O3-type HEO, a DC potentiostatic polarisation method was applied to evaluate the electronic and ionic components of electrical conductivity [6, 7]. Fig. 5S shows the polarisation curves for several polarisation voltages in the range between -0.5 and +0.5 V, recorded for  $\text{Na}_1\text{Ti}_{1/6}\text{Mn}_{1/6}\text{Fe}_{1/6}\text{Co}_{1/6}\text{Ni}_{1/6}\text{Cu}_{1/6}\text{O}_2$  HT900 at 24°C and using gold electrodes.

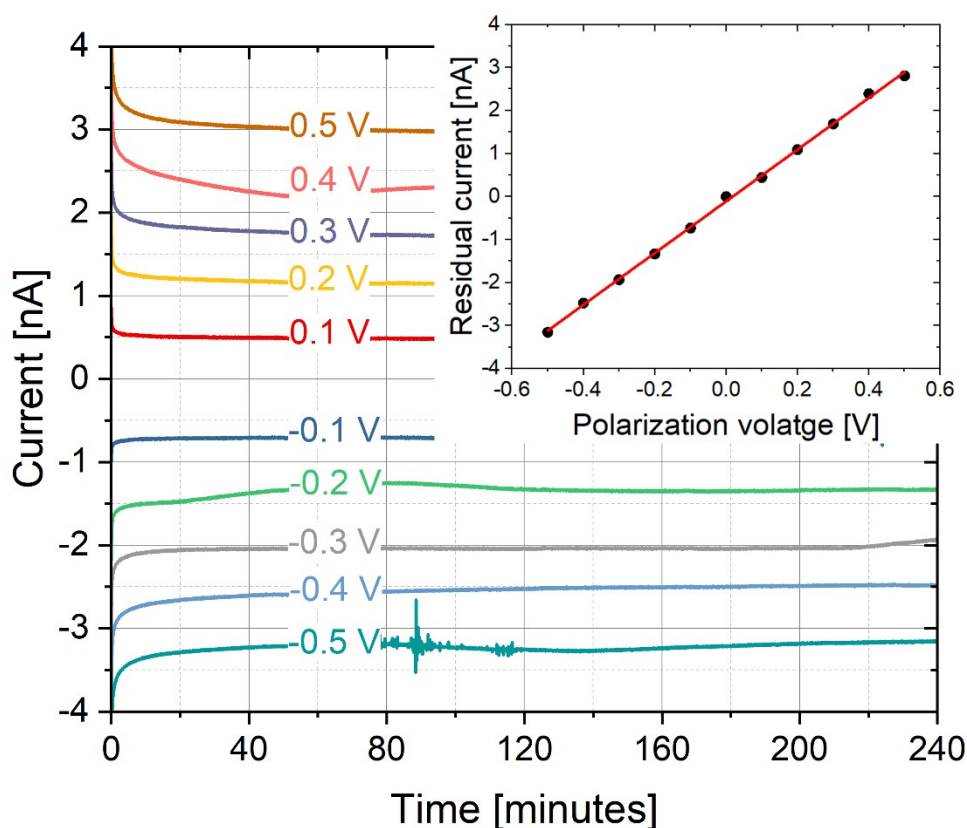


**Fig. 5S.** DC polarisation curves for  $\text{Na}_1\text{Ti}_{1/6}\text{Mn}_{1/6}\text{Fe}_{1/6}\text{Co}_{1/6}\text{Ni}_{1/6}\text{Cu}_{1/6}\text{O}_2$  HT900, recorded at  $24^\circ\text{C}$  and with Au electrodes. Inset: residual current (steady state current after 4 hours) as a function of polarisation voltage.

It was observed that after the polarisation voltage was applied, the measured current gradually decreased to reach a steady-state value after approximately 1 hour. The polarisation voltage was then kept constant for 3 more hours (total polarisation time was 4 hours) in order to confirm a steady state. The fluctuations of the measured current response over time were assumed to be due to slight fluctuations of temperature in the  $23\text{-}25^\circ\text{C}$  range. When a steady state current was achieved, the residual current flowing through the Au|sample|Au assembly was considered to be purely electronic. Moreover, the residual current changed linearly with polarisation voltage (inset in Fig. 5S), which is why it was used to estimate the electronic



## References

- [1]. C. M. Julien, A. Mauger, *AIMS Materials Science*, 5 (2018) 650.
- [2]. A. Milewska, K. Świerczek, J. Toboła, F. Boudoire, Y. Hu, D.K. Bora, B.S. Mun, A. Braun, J. Molenda, *Solid State Ionics*, 263 (2014) 110.
- [3]. C. M. Julien, A. Mauger, *AIMS Materials Science*, 5 (2018) 650.
- [4. ] F. Rahmawati, A. A. Kusumaningtyas, T. E. Saraswati, I. Yahya, Y. Lee *AIP Conference Proceedings* 2237, 020071 (2020); <https://doi.org/10.1063/5.0005348>.
- [5]. Ch. Zhou, L. Yang, Ch. Zhou, B. Lu, J. Liu, L. Ouyang, R. Hu, J. Liu, M. Zhu, *ACS Appl. Mater. Interfaces*, 11 (2019) 7906.
- [6]. J. Lu, A. Yamada, *Chem. Electro. Chem.*, 3 (2016) 902.
- [7]. M. Mozdierz, J. Dabrowa, A. Stepień, M. Zajusz, M. Stygar, W. Zajac, M. Danielewski, K. Swierczek, *Acta Materialia* 208 (2021) 116735.